Electronic Supplementary Information

Presentation of Gas-phase-reactant-accessible Single-rhodium-atom Catalysts for CO Oxidation, via MOF Confinement of an Anderson Polyoxometalate

Qin Liu,*[,a,b] Zhihengyu Chen,[c] Hafeera Shabbir,[d] Jiaxin (Dawn) Duan,[b] Wentuan Bi,[a,b] Zhiyong Lu,[b,e] Neil Schweitzer,[f] Selim Alayoglu,[f] Subhadip Goswami,[b] Karena W. Chapman,[c] Rachel B Getman,[d] Qining Wang,[b] Justin M. Notestein,[b] and Joseph T. Hupp*[,b]

[a]School of Chemistry and Materials Science, University of Science and Technology of China, Hefei 230026, China

[b]Department of Chemistry, Northwestern University, Evanston, Illinois 60208, USA

[c]Department of Chemistry, Stony Brook University, New York 11794-3400, USA

[d]Chemical and Biomolecular Engineering, Clemson University, Clemson, SC 29634, USA

[e]College of Mechanics and Materials, Hohai University, Nanjing 210098, China

[f]Department of Chemical and Biological Engineering, Center for Catalysis and Surface Science, Northwestern University, Evanston, Illinois 60208-3113, USA

Characterization and Instrumentation

Single-crystal X-ray diffraction data: Single-crystal X-ray diffraction data of $(NH_4)_3[H_6RhMo_6O_{24}]\cdot 6H_2O$ was measured on Rigaku Oxford Diffraction XtaLAB Synergy-S at 100 K using graphite monochromated Cu/Kα radiation (λ = 1.54184 Å). Data reduction was made with the Rigaku CrysAlisPro programs. The structures were solved by direct (SHELXS) and intrinsic phasing (SHELXT) methods and refined with full-matrix least squares technique using the SHELXL package. Non-hydrogen atoms were refined with anisotropic displacement parameters during the final cycles. The unit cell includes a large region of disordered solvent molecules, which could not be modeled as discrete atomic sites. We employed PLATON/SQUEEZE to calculate the diffraction contribution of the solvent molecules and thereby, to produce a set of solvent-free diffraction intensities; structures were then refined again using the data generated.

X-ray diffraction analysis: PXRD data were collected at the IMSERC X-ray Facility at Northwestern University on a STOE-STADI-MP powder diffractometer equipped with an asymmetric curved Germanium monochromator (Cu K α1 radiation, λ = 1.54056 Å) and one dimensional silicon strip detector (MYTHEN2 1K from DECTRIS). The line focused Cu Xray tube was operated at 40 kV and 40 mA. Powder was packed in a 3 mm metallic mask and sandwiched between two layers of polyimide tape. Intensity data from 2 to 30 degrees 2θ were collected over a period of 10-20 mins. The instrument was calibrated against a NIST Silicon standard (640d) prior the measurement.

Sorption studies: N_2 isotherms were measured on Micromeritics Tristar II (Micromeritics, Norcross, GA) instrument at 77 K. Pore-size distributions were obtained using a DFT carbon slit-pore model. Before each run, samples were activated at 120 °C for 24 h under high vacuum on a Smart Vacprep from Micromeritics. Around 40 mg of sample was used in each measurement.

Scanning electron microscopy (SEM): SEM images were taken using a Hitachi S-4800 at the EPIC facility (NUANCE Center-Northwestern University). Activated samples were coated with OsO_4 (~9 nm thickness) in a Denton Desk III TSC Sputter Coater before imaging.

Inductively coupled plasma optical emission spectroscopy (ICP-OES): ICP was conducted on an iCAP™ 7600 ICP-AES Analyzer (Thermo Scientific™) over the 166-847 nm spectral range. Samples (1-3 mg) were digested in a small amount (1 mL) of a concentrated nitric acid (trace metal grade) by heating in a Biotage (Uppsala, Sweden) SPX microwave reactor (software version 2.3, build 6250) at 150 °C for 15 minutes or in oil bath at 120 °C for overnight. 9 mL Millipore H_2O added to the mother solution to make 10mL. This solution was analyzed for Mo (324.754, 327.396, and 224.700 nm), Rh (324.754, 327.396, and 224.700 nm) and Zr (327.305, 339.198, 343.823, and 349.621 nm) content as compared to standard solution of 1.563, 3.125, 6.25, 12.5, 25 and 50 ppm of Mo, Rh and Zr.

^{1}H NMR Spectroscopy: Samples were prepared by weighing 2 mg of MOF into a 1.5 mL vial. About 3 to 4 drops of 0.1 M NaOD in D_2O digestion medium was then added to the vials. The vials were capped and inverted 2 or 3 times before sonicating for 30 min. This procedure dissolves only the organic portion of the MOF (linker and modulator); the inorganic component precipitates as zirconium oxide or hydroxide. To the mixture, 17 drops of D_2O were added. Then the mixture was centrifuged and the clear supernatant solution was transferred to an NMR tube. ^{1}H NMR spectra were recorded with a Bruker Avance DPX-500 NMR spectrometer (500 MHz; 64 scans).

Diffuse reflectance infrared Fourier transform (DRIFT) spectra: were recorded on a Nicolet 7600 FTIR spectrometer equipped with an MCT/A detector. Samples diluted in KBr were measured with a KBr background and kept at each temperature under Ar purge (samples prepared in atmosphere). The spectra were collected at 1 cm^{-1} resolution and 64 scans were averaged over the spectral window of 650-4000 cm^{-1}. All spectra were collected after heating at 125°C overnight in Argon.

X-ray photoelectron spectroscopy (XPS): XPS measurements were carried out at the KECK-II/NUANCE facility at Northwestern University on a Thermo Scientific ESCALAB 250 Xi (Al Kα radiation, hν = 1486.6 eV) equipped with an electron flood gun. All spectra from XPS were analyzed as reference to the C 1s peak (284.8 eV) by using Thermo Scientific Advantage Data System software.

Synchrotron X-ray Experiments: High-energy X-ray scattering data were collected at beamline 11-ID-B, for Pair Distribution Function (PDF) analysis, and at beamline 17-BM, for Differential Envelope Density (DED) analysis, at the Advanced Photon Source, Argonne National Laboratory. Images were acquired using an area detector with X-ray wavelengths of 0.2114 Å for PDF and 0.4524 Å for DED. 2D diffraction images were integrated to 1D data within GSAS-II.[1] PDFs were extracted using xPDFsuite.[2] PDFs were modeled within PDFgui.[3] The DED was calculated described previously[4] and visualized within Chimera.[5]

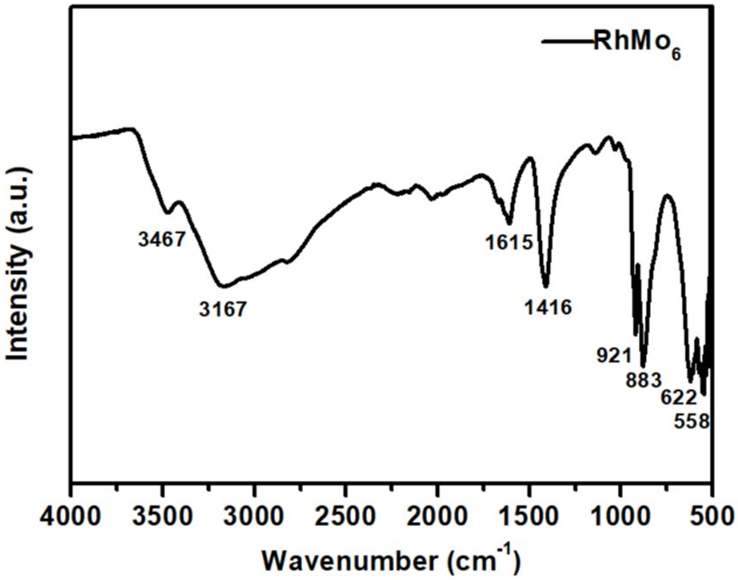

Supplementary Fig. 1 FT-IR spectra of $RhMo_6O_{24}$. The broad peaks located at 3467 cm^{-1} and 3167 cm^{-1}can be ascribed to the stretching vibration of the NH and OH groups. The peaks at 1615 cm^{-1} and 1416 cm^{-1} can be attributed to the bending vibration of OH and NH, respectively. The peaks at 921 cm^{-1} and 883 cm^{-1} are associated with the Mo=O stretching vibrations. The peaks at 622 cm^{-1} and 558 cm^{-1} are attributed to asymmetric Mo-O-Mo and Rh-O-Mo stretching vibrations, respectively.[6]

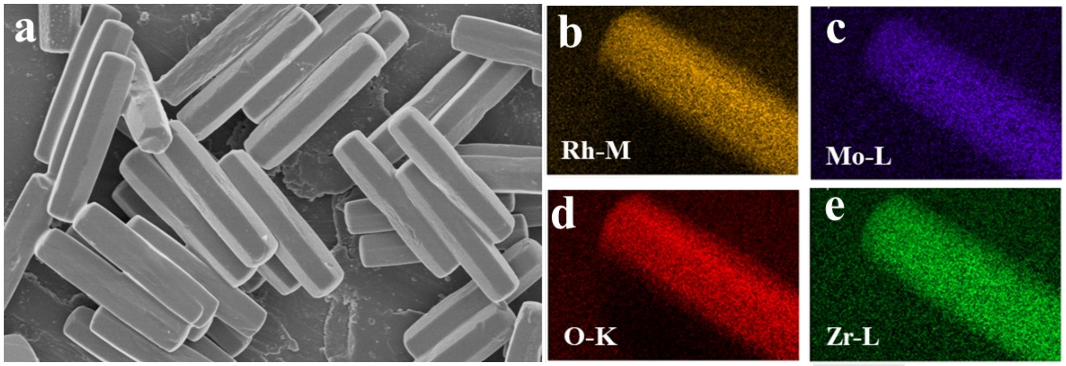

Supplementary Fig. 2 (a) SEM and (b-e) EDS mapping of NU1K after $RhMo_6O_{24}$ incorporation, indicating the homogeneous distribution of rhodium, molybdenum, oxygen, and zirconium.

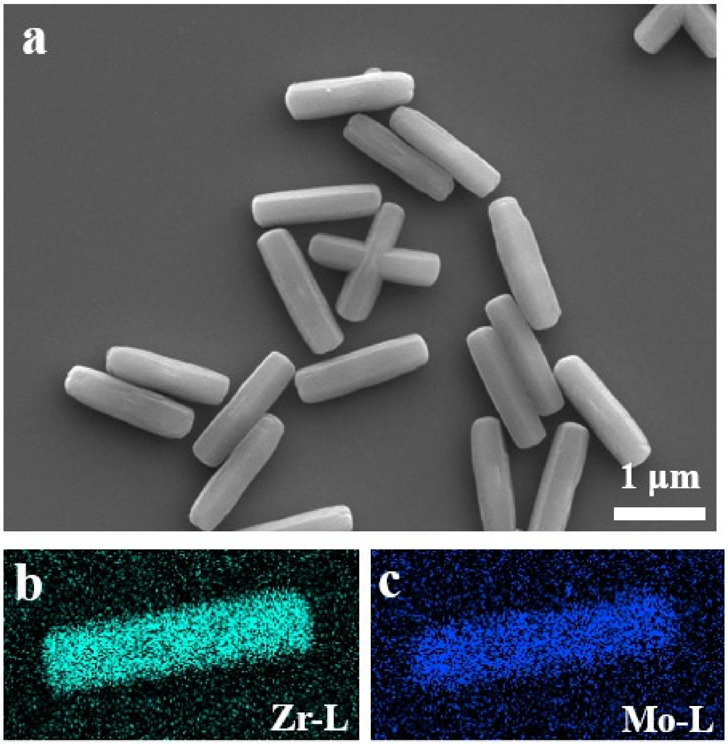

Supplementary Fig. 3 (a) SEM and (b-c) EDS mapping of Mo_7O_{24}@NU1K, indicating the homogeneous distribution of molybdenum and zirconium.

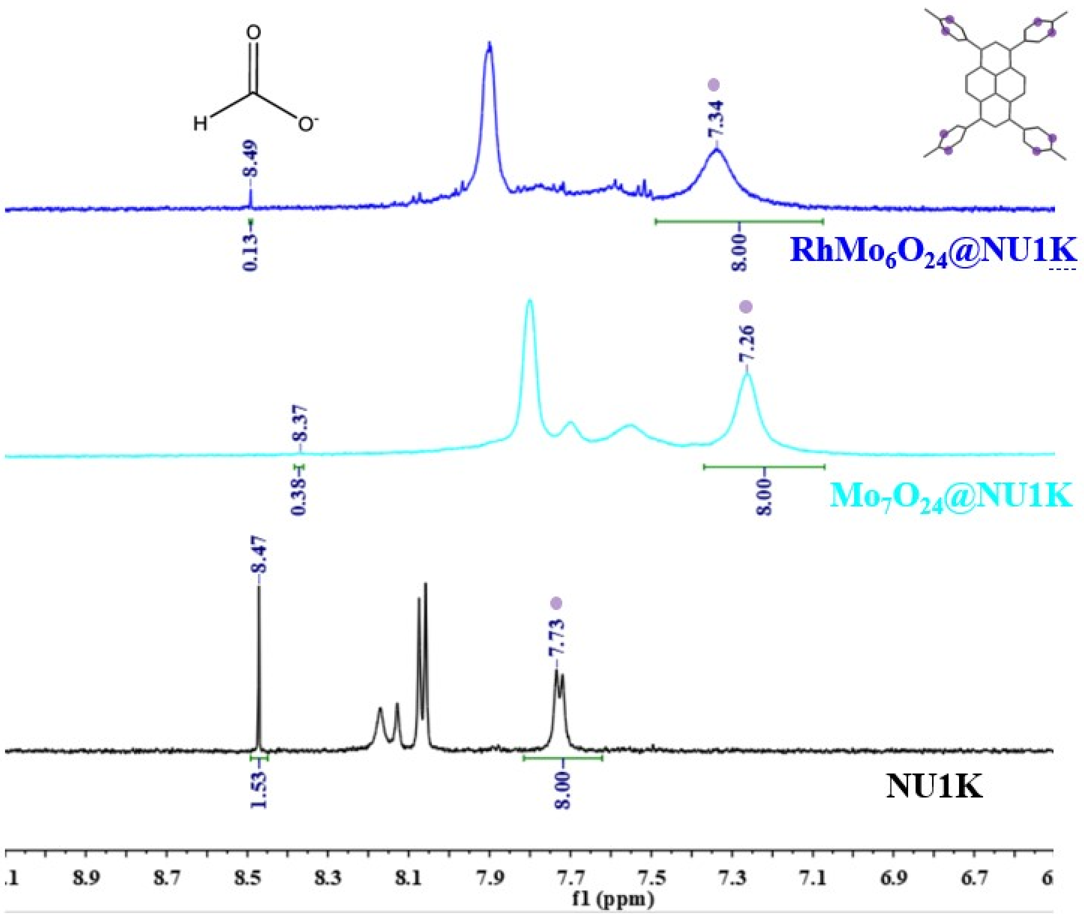

Supplementary Fig. 4 (a) ^{1}H NMR spectra showing the successful POM replacement of formate.

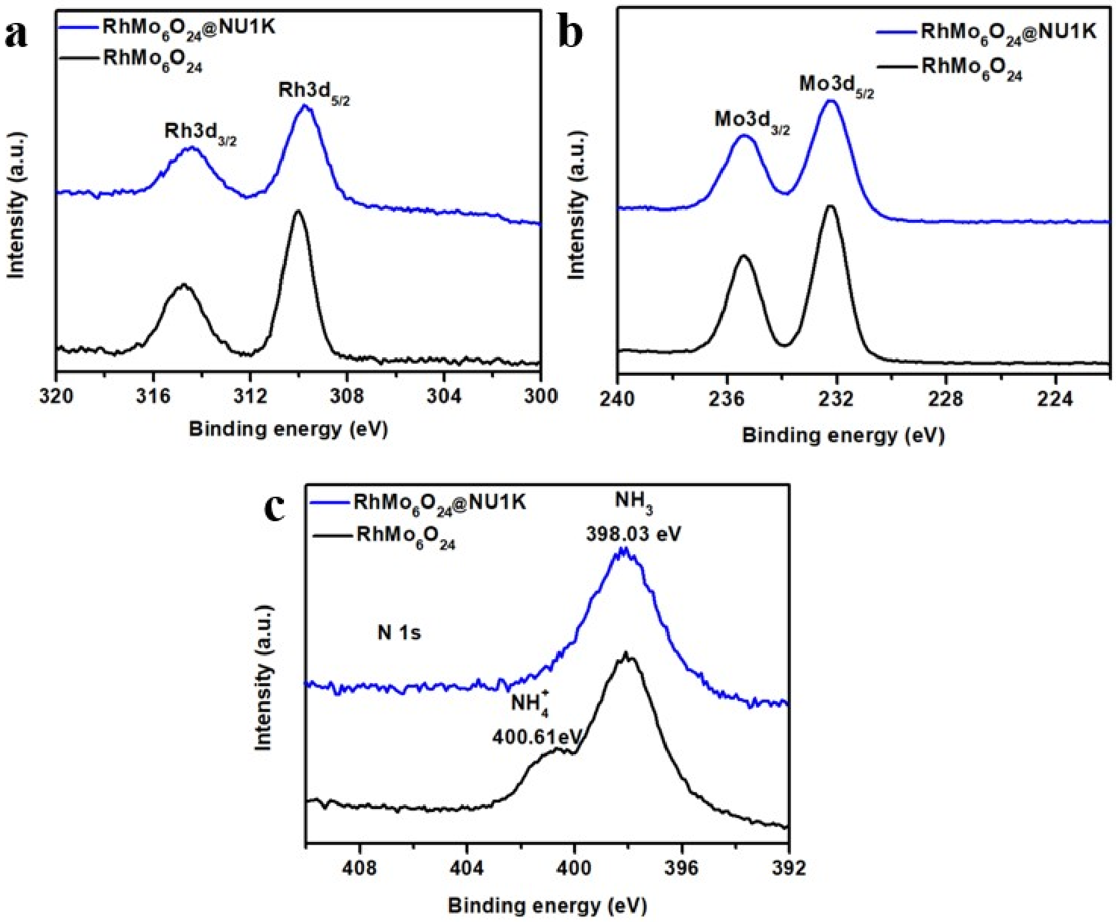

Supplementary Fig.5 In the high-resolution XPS spectra of Rh (a), peaks for Rh 3d$_{5/2}$ and Rh 3d$_{3/2}$ are located at 73.9 and 77.3 eV, respectively, which are in accordance with the presence of Rh(III) (reference 39 in maintext). In the high-resolution XPS spectra of Mo (b), peaks for Mo 3d$_{5/2}$ and Mo 3d$_{3/2}$ are located at 232.24 and 235.40 eV, respectively, which are in accordance with the presence of Mo(VI). The XPS spectra of N 1s is depicted in (c), the peaks at 398.03 and 400.61 eV belong to NH_3 and NH_4^+, respectively.[7]

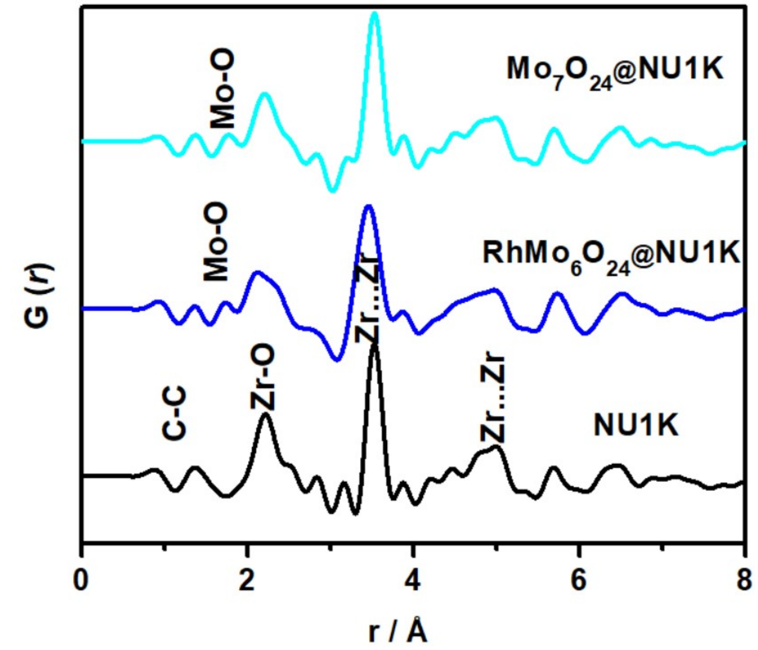

Supplementary Fig. 6 PDFs of NU1K, Mo_7O_{24}@NU1K and $RhMo_6O_{24}$@NU1K.

Determination of activation energy (E_a)

All reactivity studies were carried out using a packed bed reactor in the REACT core facility at Northwestern University. In a typical reaction, ~20 mg of catalyst was diluted with 1 g of silica (trace-metal grade) and packed in a quartz tube. The height of the bed was approximately 0.8 cm. The reaction temperature was controlled with a K-type thermocouple at the top of the catalyst bed. Pressure in the reactor was monitored to be ~10 psig (~ 0.68 atm) using a back-pressure regulator directly downstream from the reactor. The temperatures were heated to 110°C, and a pre-mixed gas stream of 0.1% CO/10% O_2 balanced in N_2 was then flowed over the sample. For kinetic studies, 5 temperature points, 110°C, 130°C, 160°C, 190°C, 220°C, were measured. Products were analyzed via gas chromatography-flame ionization detection (GC-FID), and the gas mixture downstream were separated using a GS-Gaspro column (Agilent, 30m length, 0.32 mm diameter).

Reaction rates were calculated by multiplying the molar flow rate by the conversion under each reaction condition and then normalizing to the moles of Rh (mol CO_2*mol^{-1} Rh). The molar flow rate of CO, $n(CO)$ in mmol*s^{-1}, was calculated using ideal gas law:

$$n(CO) = \frac{(\frac{20}{60}\,mL * s^{-1})(1.68\ atm)}{(0.0821\ atm * \frac{L}{mol} * k)(T\ (k))}$$

where T is the reaction temperature.

To extract the activation energy of the catalyst for CO oxidation, Ea, ln(rate) was plotted against 1000/T, and a linear regression was obtained from the plot in **Supplementary Fig. S7**. According to the Arrhenius equation:

$$\ln(rate) = -\frac{Ea}{RT} + \ln(A)$$

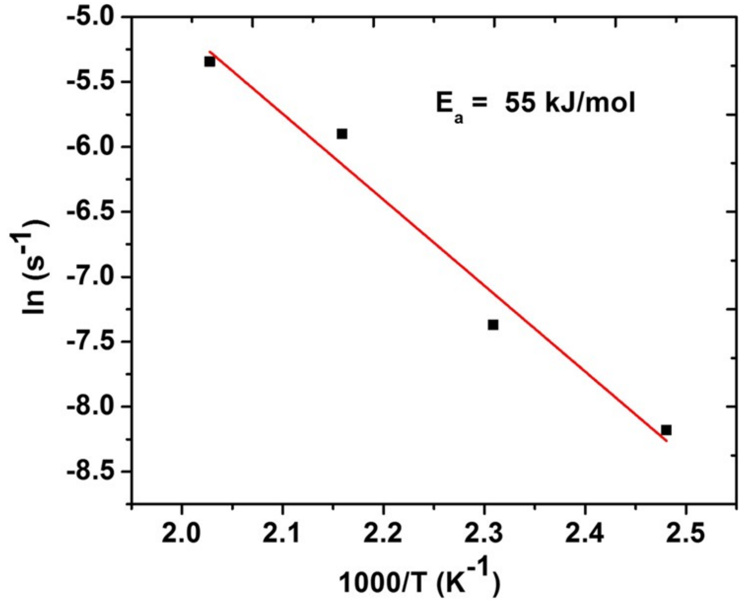

Supplementary Fig. S7 Arrhenius plot for CO oxidation catalyzed by $RhMo_6O_{24}$@NU1K

	$(NH_4)_3[H_6RhMo_6O_{24}]\cdot 6H_2O$
Formula weight	1230.79
Cystal system	monoclinic
Space group	$P2_1/c$
a [Å]	11.3661(4)
b [Å]	10.9443(3)
c [Å]	11.7564(3)
α [Å]	90
β [Å]	100.180(3)
γ [Å]	90
V [Å^3]	1439.40(8)
Z	6
Temperature [K]	99.98(15)

Supplementary Table 1. Crystal data of $(NH_4)_3[H_6RhMo_6O_{24}]\cdot 6H_2O$

Computational Details:

Geometry relaxations were performed using the Gaussian 09 software[8] using the default convergence criteria. Electron exchange and correlation were modeled using the M06-L[9,10] density functional. All structures were optimized with the Def2-SVP basis set for H, C, and O atoms and the Def2-TZVPP basis set with the associated effective core potential for Mo and Rh.[11,12] All structures were confirmed to be minima on the potential energy surface by frequency computation. The CO vibrational frequencies were also taken from the frequency calculations. The coordinates of the computed structures are given in SI table S3.

The two catalysts models with formulas $[RhMo_6O_{22}H_6(CO)_2]^{1-}$ and $[RhMo_6O_{22}H_7(CO)_2]$ given in **Figure S8** where Rh is in +1 oxidation state were evaluated in Gaussian 09. Two spin states (singlet and triplet) for both models were evaluated. The singlet structures gave the lowest energies. The scaled frequencies of the singlet structures give good agreement with the experimental values (2027 cm^{-1}, 2093 cm^{-1}). The computed IR frequencies of the 2 CO molecules in these structures are given with experimental IR frequencies in **Figure 4c**. The frequencies have been scaled by a factor of 0.976.[13] The $[RhMo_6O_{22}H_6(CO)_2]^{1-}$ and $[RhMo_6O_{22}H_7(CO)_2]$ give very similar symmetric (2051 cm^{-1}, 2061 cm^{-1}) , and anti-symmetric frequencies (2115 cm^{-1}, 2124 cm^{-1}) in line with what is expected of the supported single atom rhodium dicarbonyl $Rh(CO)_2$.[14-16] Models with stoichiometry $[RhMo_6O_{22}H_6(CO)_2]^{3-}$ and $[RhMoO_6O_{22}H_9(CO)_2]$ where Rh is in +3 oxidation state were also evaluated but the frequencies were found to be much lower than the models with Rh in +1 oxidation state.

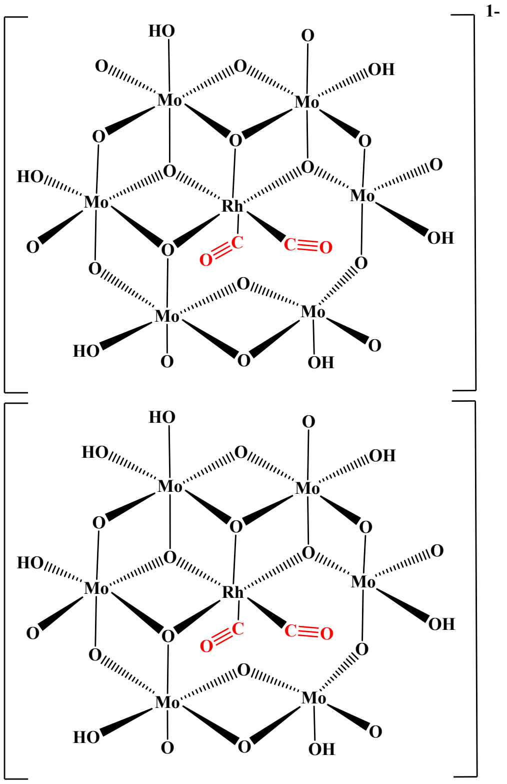

$[RhMo_6O_{22}H_6(CO)_2]^{1-}$ $[RhMoO_6O_{22}H_7(CO)_2]$

Supplementary Fig. 8 Two catalyst models evaluated in Gaussian 09.

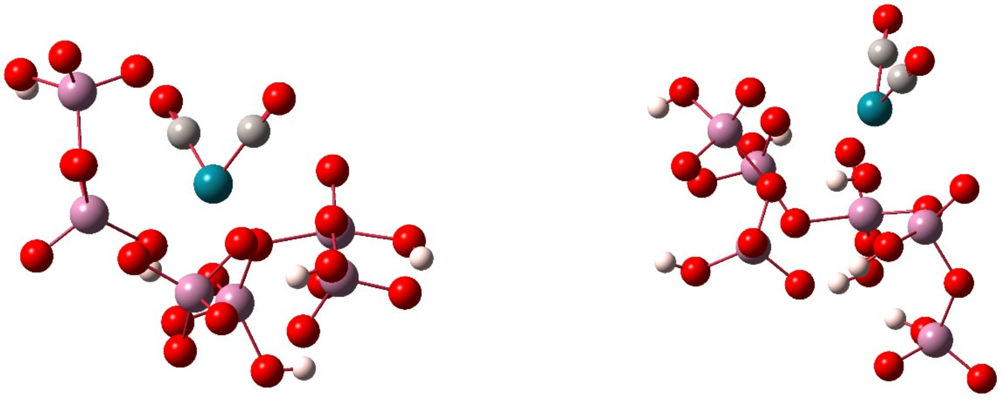

Supplementary Fig. 9 $[RhMo_6O_{22}H_6(CO)_2]^{1-}$ singlet(left) and $[RhMoO_6O_{22}H_7(CO)_2]$ singlet (right) representation in Gaussview. Rh= Teal Mo=Pink O=red C=red H= white.

Supplementary Table 2. Calculated IR Frequencies scaled by 0.976 and experimental values for comparison.

Structure	$[RhMo_6O_{22}H_6(CO)_2]^{1-}$	$[RhMoO_6O_{22}H_7(CO)_2]$	Experimental
singlet	2051 cm^{-1}, 2115 cm^{-1}	2060 cm^{-1}, 2124 cm^{-1}	2027 cm^{-1}, 2093 cm^{-1}
triplet	2012 cm^{-1}, 2056 cm^{-1}	2102 cm^{-1}, 2150 cm^{-1}	

Supplementary Table 3. Co-ordinates of the DFT optimized structures in xyz format

39

$[RhMo_6O_{22}H_6(CO)_2]^{1-}$ Singlet

Mo	-0.246278611	2.112589316	1.352998069
Mo	2.441299634	-1.818450879	1.725501162
Mo	-4.973135954	-0.250210569	-1.072717752
Mo	-2.869609841	-0.100386223	1.405280301
Mo	2.720474622	2.113062358	-0.877234997
Mo	3.294061107	-1.221690603	-1.279823672
O	0.587635579	1.518490176	2.898781385
O	0.068825590	3.773495959	1.259870522
O	-2.013238020	1.882889238	1.435352124
O	-3.379328753	-0.122358978	3.003720321
O	3.983913518	-1.260721999	2.678144753
O	2.282020909	-3.494881227	1.792042291
O	1.206655017	-1.167106239	2.771796053
O	4.763824333	-0.416976882	-2.145124448
O	1.759082663	-1.210281235	0.076925790

O	0.302767743	1.468348090	-0.228765905
O	-3.801437082	-0.643481226	-2.231034045
O	-6.164315342	0.671585013	-1.827741749
O	-5.845316579	-1.799333543	-0.436642897
O	-3.274686405	-1.646710999	0.774251281
O	-0.878145341	-0.429181782	1.337840703
O	-4.176342581	0.784068148	0.298595891
O	2.363194079	0.496838235	-1.714771306
O	2.867622674	1.852468412	0.799724507
O	4.295029541	2.414979149	-1.460939324
O	1.731084331	3.663618974	-1.299399091
O	2.833525956	-2.465163987	-2.311750021
O	4.126536444	-1.890941071	0.128573273
Rh	-0.463332019	-0.409337560	-0.820088971
H	0.877810266	0.579332979	3.001918875
H	1.039801760	3.922315164	-0.665197421
H	4.902477562	0.547149410	-2.099978414
H	4.793986572	-1.362868235	2.158983223
H	-5.223482997	-2.467145787	-0.106256739
H	-0.309860274	-0.944114969	1.963353045
C	-0.583948732	0.065137527	-2.580031779
O	-0.660202776	0.395165600	-3.678655878
O	-1.693330141	-3.028843247	-1.541798988

C	-1.236027104	-2.013230484	-1.261453449

39

$[RhMo_6O_{22}H_6(CO)_2]^{1-}$ Triplet

Mo	-0.778771857	2.335749642	0.397925045
Mo	2.357856416	-0.797796269	2.203846327
Mo	-4.309980766	-0.528967030	-1.269070574
Mo	-3.172462746	0.214663370	1.466522233
Mo	2.555396792	1.817421079	-1.338976778
Mo	3.380822081	-1.333770987	-0.764887205
O	0.072188610	2.588131953	2.027498975
O	-0.647350850	3.844663584	-0.374938820
O	-2.558586180	1.981198007	0.582854124
O	-3.690744677	0.527789315	3.030192914
O	3.823575681	0.120331974	2.983214890
O	2.223734812	-2.298103028	2.956632837
O	1.059081247	0.160678523	2.845946279
O	4.856010046	-0.745854224	-1.781265719
O	1.725869903	-1.053419040	0.413187801
O	0.067210881	1.227998247	-0.679381772
O	-2.585894063	-0.374438883	-1.400775124
O	-5.063236925	0.055213377	-2.657903259
O	-4.847004878	-2.327254601	-1.081962673
O	-3.358782263	-1.480922283	1.176552528

O	-1.175337992	0.081123374	1.442387614
O	-4.705082208	0.522484997	0.188300903
O	2.355381248	0.031219775	-1.807151501
O	2.649265351	1.849955249	0.365387485
O	4.141948730	2.100956117	-1.899304828
O	1.536849614	3.180979943	-2.135235729
O	3.124400115	-2.904706762	-1.304294684
O	4.124846437	-1.338590018	0.841537481
Rh	-0.401071905	-1.034303540	-0.508744145
H	0.532325368	1.813766227	2.435907710
H	0.734024235	3.528486229	-1.698415401
H	4.954778691	0.202401371	-1.986942061
H	4.662575683	-0.079030795	2.545648369
H	-4.405684824	-2.739920397	-0.319477520
H	-0.597573061	-0.104133350	2.216687659
C	0.092920110	-1.584064551	-2.288062139
O	0.312858966	-2.096869355	-3.291211128
O	-1.398979409	-3.858775634	0.054747700
C	-1.017937555	-2.771739881	0.043873
40			
$[RhMoO_6O_{22}H_7(CO)_2]$ Singlet			
Mo	-1.159332774	1.076940385	1.371996489
Mo	1.177255445	-3.018056933	-0.546696990

Mo	-4.644962396	-1.035777039	0.342479129
Mo	-2.226027811	0.463933078	-1.499052545
Mo	1.946734119	0.267750603	1.918037463
Mo	3.751098449	-0.843232689	-0.567387719
O	-2.056975024	-0.640048597	0.611444510
O	-1.948581154	1.282115639	2.837915105
O	-2.264868106	1.733905359	0.032069227
O	-1.602444770	-1.130597255	-2.191418384
O	1.835903541	-4.023615826	0.884689966
O	1.512260898	-3.730328746	-2.027889280
O	-0.529083477	-2.884561462	-0.387677193
O	5.134100580	-0.175155484	0.523217895
O	1.757147605	-1.238928032	-0.554412505
O	0.228747735	2.234628650	1.366312861
O	-4.031116067	-2.604424848	0.350098183
O	-6.287701475	-1.167178037	0.039580190
O	-4.562884825	-0.155627469	1.996738259
O	-2.254691409	1.468892704	-2.825358704
O	-0.183704949	0.753368446	-0.888559644
O	-3.972297094	-0.013315389	-1.189192957
O	2.594435009	0.934537941	0.431540160
O	0.218864530	-0.332422115	1.820916559
O	2.935168769	-1.081028258	2.194998649

O	2.195781540	1.416965190	3.362434818
O	4.071562282	-0.220628671	-2.087278548
O	4.049809638	-2.519469692	-0.614419851
Rh	0.741331379	2.675088395	-0.696453717
H	-1.574663977	-1.484187856	0.686244063
H	1.743656729	2.274907455	3.324121796
H	5.314791662	-0.630746561	1.357157968
H	2.691863609	-4.468754434	0.802800323
H	-3.766692439	-0.171115708	2.548381839
H	0.458821315	0.020438777	-1.000929334
C	1.419441448	4.342446888	-0.358356651
O	1.840606021	5.384636545	-0.123559630
O	1.016906517	3.170155756	-3.621404296
C	0.927921326	2.991088041	-2.491465972
H	-1.367567752	-1.901151080	-1.618491709

40

[$RhMoO_6O_{22}H_7(CO)_2$] Triplet

Mo	0.931744859	1.776882025	-1.222687372
Mo	-2.181652577	-2.501870433	-0.956001374
Mo	4.582953908	0.306390053	0.888424936
Mo	2.896393118	-1.149346782	-0.873720716
Mo	-2.216784461	2.666083598	-0.162489938
Mo	-3.739002781	-0.318420808	0.784592007

O	0.572139793	0.917882919	-2.886406883
O	0.954575791	3.463657936	-1.333413855
O	2.568607733	1.238602413	-0.995896446
O	2.698790533	-1.015458910	-2.741518465
O	-3.369645821	-3.622976672	-1.892319673
O	-1.254842957	-3.573188876	-0.032952058
O	-1.153343403	-1.863758863	-2.174043861
O	-5.134982623	0.838926123	0.356295467
O	-1.910435938	-0.954312716	0.302110197
O	0.058455859	1.459424332	0.364936485
O	2.913581831	-0.343762296	1.133763645
O	4.722803966	1.968212019	1.055835290
O	5.791833961	-0.469621225	2.085604908
O	3.191252252	-2.747266028	-0.527569984
O	0.885771636	-0.940350762	-0.683192563
O	4.832064523	-0.314355271	-0.783983750
O	-2.635983638	1.327856791	1.037438179
O	-1.556175224	2.060116966	-1.642304276
O	-3.769481848	3.232098573	-0.537005411
O	-1.252680734	4.110939083	0.515485596
O	-4.020195579	-0.898192045	2.329366870
O	-4.062616234	-1.660620771	-0.379385796
Rh	0.063722353	-0.429315813	1.187033544

H	-0.309527478	1.054589786	-3.264180020
H	-0.333961367	4.215569022	0.207039038
H	-5.060850828	1.733799989	-0.025739407
H	-4.320841747	-3.462005188	-1.849119741
H	5.940387127	-1.425018621	2.115024203
H	0.252982141	-1.295431590	-1.363455764
C	-0.596925941	0.236227518	2.812511535
O	-1.010182405	0.655243100	3.788815920
O	0.579609394	-3.153017023	2.408902760
C	0.332900982	-2.147583852	1.933709824
H	1.943702203	-0.510925871	-3.102841435

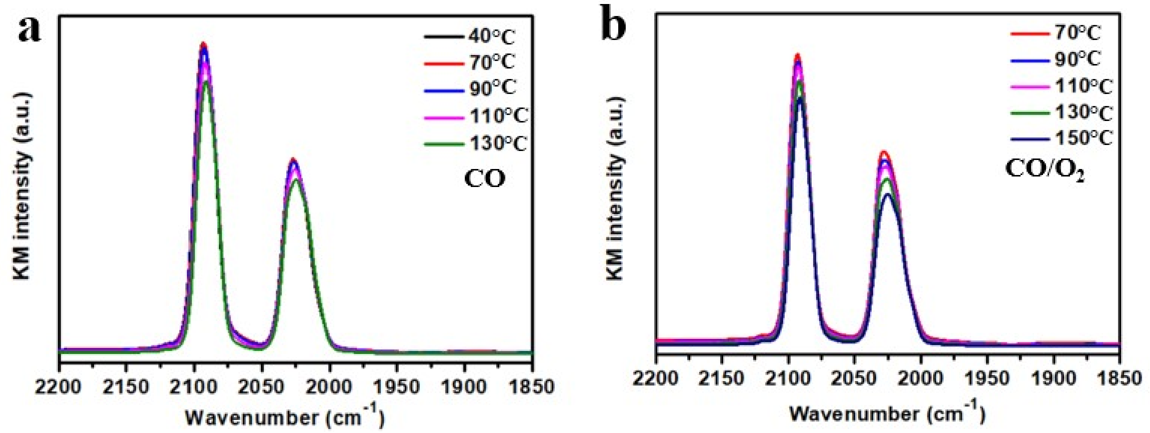

Supplementary Fig. 10 (a) Temperature-dependent diffuse reflectance infrared Fourier transform spectroscopy (DRIFTS) peak intensity reduction (due to CO desorption) for samples with only surface-adsorbed CO in flowing Ar. DRIFTS results for (b) $RhMo_6O_{24}$@NU1K with both surface-adsorbed CO and O_2 in flowing Ar at various temperatures.

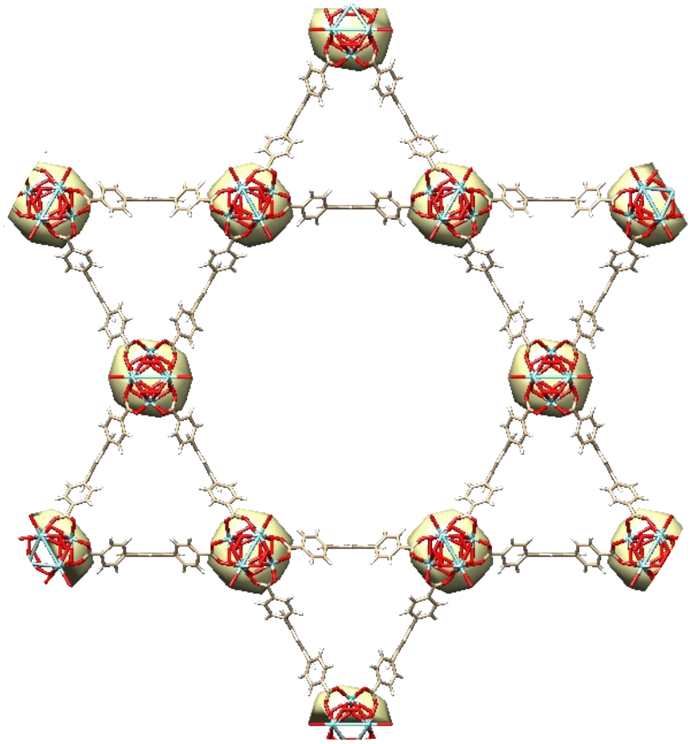

Supplementary Fig. 11 DEDs corresponding to the location of (a) $RhMo_6O_{24}$@NU1K after catalysis in electron density viewed parallel to the c-axis.

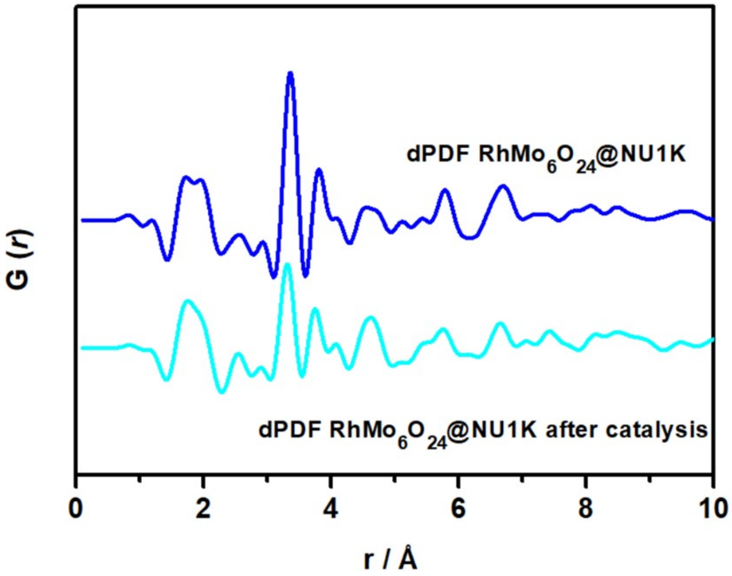

Supplementary Fig. 12 Differential PDFs of $RhMo_6O_{24}$@NU-1K before and after catalysis. The d-PDF does not change significantly during the reaction, with exception of a contraction of the Mo…Mo/Rh from 3.36 Å to 3.30 Å.

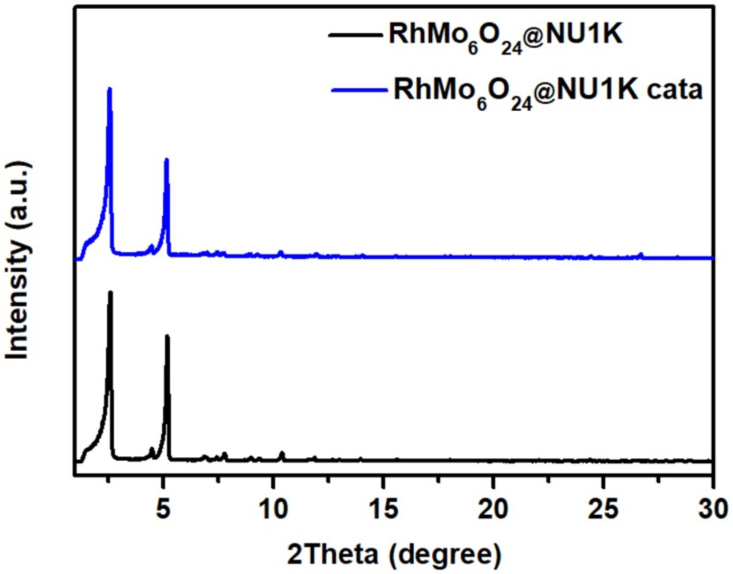

Supplementary Fig. 13 PXRD patterns for $RhMo_6O_{24}$@NU1K after CO oxidation reaction, indicating the structure of NU1K was well maintained.

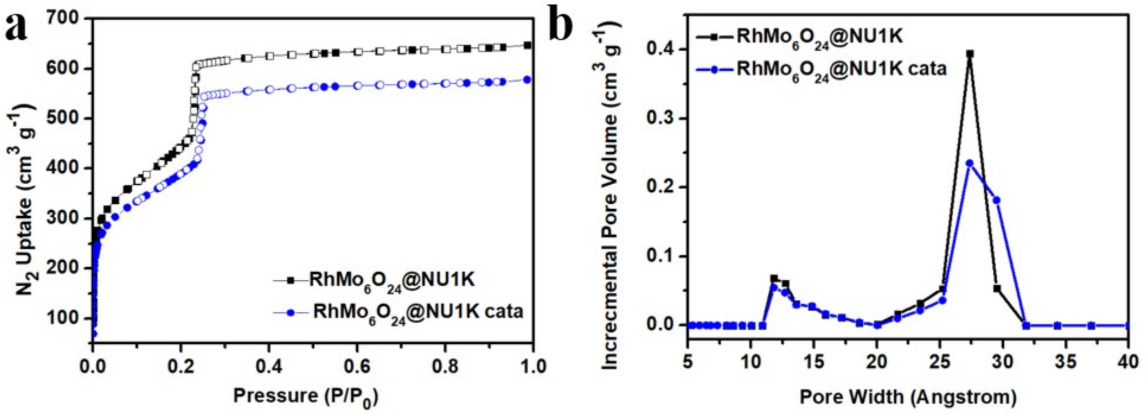

Supplementary Fig. 14 (a) and (b) are volumetric N_2 isotherm (above) and pore size distribution (below) of $RhMo_6O_{24}$@NU1K after catalysis.

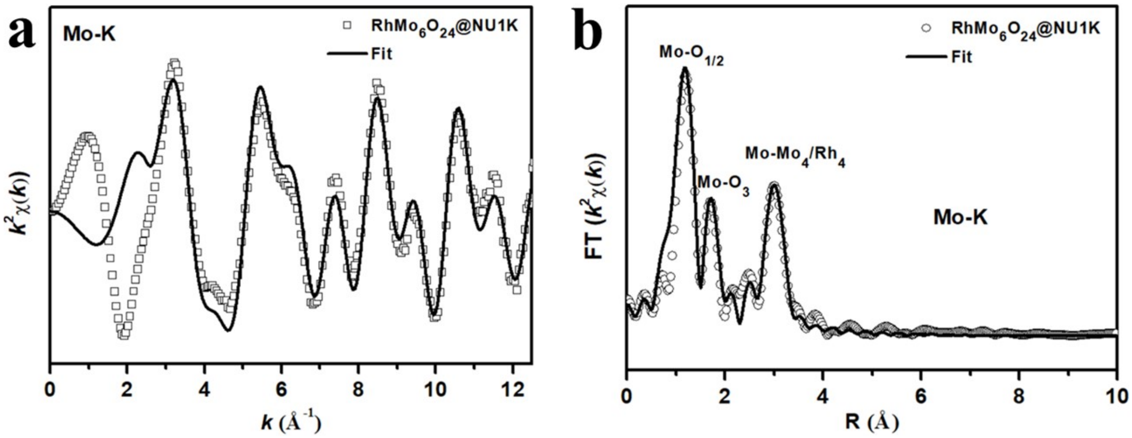

Supplementary Fig. 15 Fitting curves for EXAFS data at the Mo K-edge for $RhMo_6O_{24}$@NU1K. The data are k^2-weighted and not phase-corrected.

Path	*R* (Å)	*N*	△E_0 (eV)	σ^2 (Å^2)
Mo-O_1	1.70	**2.0**	-3.4	0.002
Mo-O_2	1.95	**2.0**	-3.4	0.008
Mo-O_3	2.32	**2.0**	-0.1	0.006
Mo-Mo_4/Rh_4	3.35	**3.0**	-3.0	0.006

Supplementary Table 4. Local structural parameters for Mo atoms in $RhMo_6O_{24}$@NU1K fitted from EXAFS data. The structure of $RhMo_6O_{24}$@NU1K is fit with $RhMo_6O_{24}$ well.

R is the length of bond, N is the coordination number, σ^2 is Debye-Waller factor and ΔE_0 is the edge-energy shift. Bold numbers indicate fixed coordination number (N) according to the crystal structure. The numbers in the lower right corner of each path are the corresponding shells.

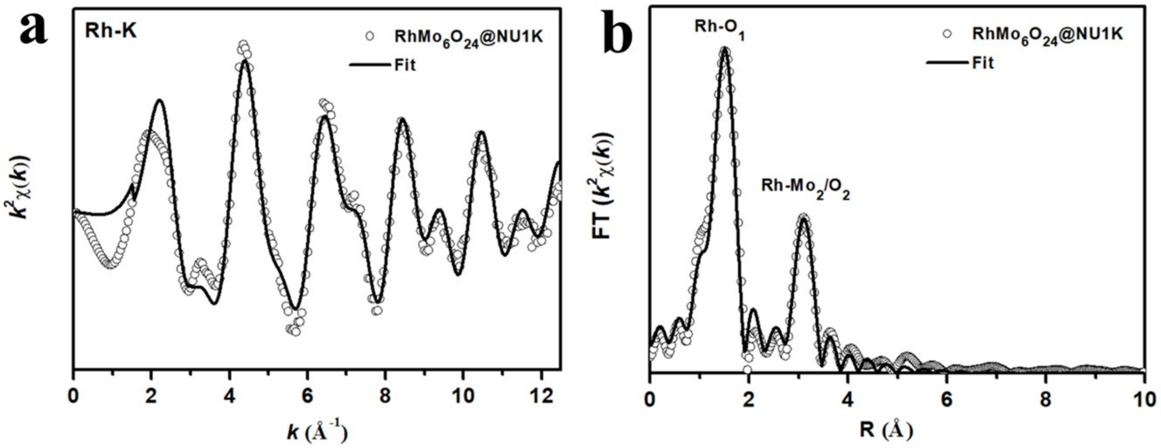

Supplementary Fig. 16 Fitting curves for EXAFS data at the Rh K-edge for $RhMo_6O_{24}$@NU1K. The data are k^2-weighted and not phase-corrected.

Path	R (Å)	N	△E_0 (eV)	σ^2 (Å^2)
Rh-O_1	2.02	**6.0**	-1.7	0.002
Rh-Mo_2	3.40	**6.0**	-1.0	0.005
Rh-O_2	3.48	**6.0**	8.7	0.008

Supplementary Table 5. Local structural parameters for Rh atom in $RhMo_6O_{24}$@NU1K after catalysis fitted from EXAFS data. The structure of $RhMo_6O_{24}$@NU1K is fit with $RhMo_6O_{24}$ well.

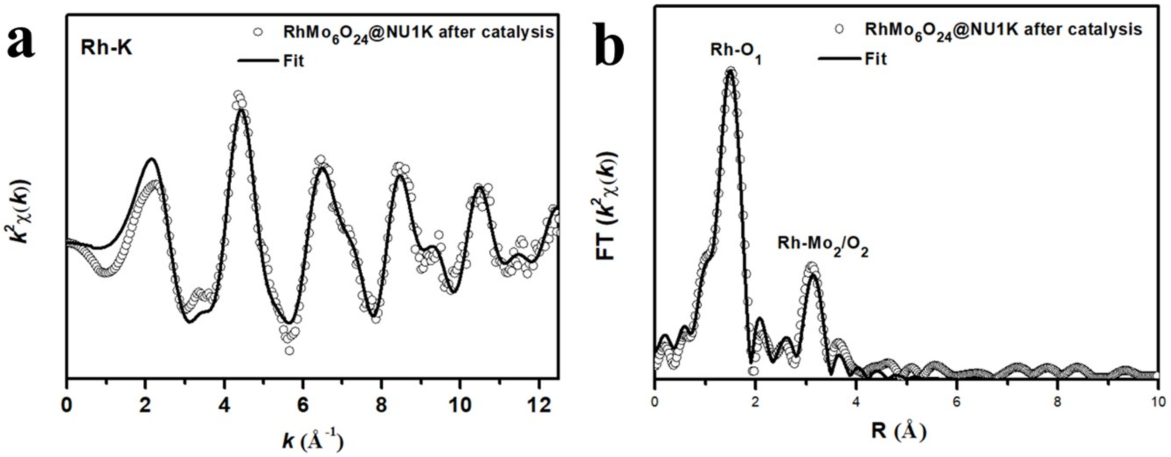

Supplementary Fig. 17 Fitting curves for EXAFS data at the Rh K-edge for $RhMo_6O_{24}$@NU1K after catalysis. The data are k^2-weighted and not phase-corrected.

Path	*R* (Å)	*N*	△E_0 (eV)	σ^2 (Å^2)
Rh-O_1	2.01	**6.0**	-2.9	0.002
Rh-Mo_2	3.40	**6.0**	1.4	0.007
Rh-O_2	3.33	**6.0**	1.4	0.011

Supplementary Table 6. Local structural parameters for Rh atom in $RhMo_6O_{24}$@NU1K after catalysis fitted from EXAFS data. The structure of $RhMo_6O_{24}$@NU1K is fit with $RhMo_6O_{24}$well.

To obtain structural parameters around Mo and Rh atoms in $RhMo_6O_{24}$@NU1K, the least-squares curve parameter method was used with the ARTEMIS module of IFEFFIT software packages.[17] Effective scattering amplitudes and phase-shifts of Mo-O, Mo-Mo/Rh, Rh-O and Rh-Mo/O bonds were calculated with the ab initio code FEFF8.0.[18] The coordination numbers in the all-coordination shells of the $RhMo_6O_{24}$@NU1K were fixed to the nominal values according to structural data of Table S1. Bold numbers are parameters that are fixed in the fit. The interatomic distances R and other parameters were left free. The amplitude reduction factor S_0^2 was fixed as 0.908 in the fit at the Rh K-edge in the spectrum of the $RhMo_6O_{24}$@NU1K. The amplitude reduction factor S_0^2 was fixed as 0.8 in the fit at the Rh K-edge in the spectrum of the $RhMo_6O_{24}$@NU1K results after catalysis are in excellent agreement with crystallographic values, showing the high accuracy of EXAFS in the determination of structural parameters. We got a closest match between the simulated and experimental spectra as shown in Supplementary Fig. 15-17. The obtained parameters are listed in above.

References

(1) Toby, B. H.; Von Dreele, R. B. GSAS-II: The Genesis of a Modern Open-Source All Purpose Crystallography Software Package. *J. Appl. Crystallogr.* **2013,** *46,* 544-549.

(2) Yang, X.; Juhas, P.; Farrow, C. L.; Billinge, S. J. L. XPDF suite: An End-to-End Software Solution for High Throughput Pair Distribution Function Transformation, Visualization and Analysis. **2014,** 1-4.

(3) Farrow, C. L.; Juhas, P.; Liu, J. W.; Bryndin, D.; Boin, E. S.; Bloch, J.; Proffen, T.; Billinge, S. J. L. PDFfit2 and PDFgui: Computer Programs for Studying Nanostructure in Crystals. *J. Phys. Condens. Matter* **2007,** *19,* 1-7.

(4) Yakovenko, A. A.; Wei, Z.; Wriedt, M.; Li, J. R.; Halder, G. J.; Zhou, H. C. Study of Guest Molecules in Metal-Organic Frameworks by Powder X-Ray Diffraction: Analysis of Difference Envelope Density. *Cryst. Growth Des.* **2014,** *14,* 5397-5407.

(5) Pettersen, E. F.; Goddard, T. D.; Huang, C. C.; Couch, G. S.; Greenblatt, D. M.; Meng, E. C.; Ferrin, T. E. UCSF Chimera - A Visualization System for Exploratory Research and Analysis. *J. Comput. Chem.* **2004,** *25,* 1605-1612.

(6) Huang, Y.; Sun, Y.; Zheng, X.; Aoki, T.; Pattengale, B.; Huang, J.; He, X.; Bian, W.; Younan, S.; Williams, N.; Hu, J.; Ge, J.; Pu, N.; Yan, X.; Pan, X.; Zhang, L.; Wei, Y.; Gu, J. Atomically engineering activation sites onto metallic 1T-MoS_2 catalysts for enhanced electrochemical hydrogen evolution. *Nat. Commun.* **2019,** *10,* 1-11.

(7) Liu, Q.; Li, X.; He, Q.; Khalil, A.; Liu, D.; Xiang, T.; Wu, X.; Song, L. Gram-Scale Aqueous Synthesis of Stable Few-Layered 1TMoS_2: Applications for Visible-Light - Driven Photocatalytic Hydrogen Evolution. *Small* **2015,** *11,* 5556-5564.

[8] Frisch, J. M.; Trucks, W. G.; Schlegel, B. H.; Scuseria, E. G.; Robb, A. M.; Cheeseman, R. J.; Scalmani, G.; Barone, V.; Petersson, A. G.; Nakatsuji, H.; Li, X.; Caricato, M.; Marenich, A.; Bloino, J.; Janesko, G. B.; Gomperts, R.; Mennucci, B.; Hratchian, P. H.; Ort, V. J.; F. B. J.; F. J. D. Gaussian 09. Gaussian, Inc.: Wallingford CT 2016.

[9] Zhao, Y.; Truhlar, D. G. A New Local Density Functional for Main-Group Thermochemistry, Transition Metal Bonding, Thermochemical Kinetics, and Noncovalent Interactions. *J. Chem. Phys.* **2006**, *125*, 194101-194118.

[10] Zhao, Y.; Truhlar, D. G. Density Functionals with Broad Applicability in Chemistry. *Acc. Chem. Res.* **2008**, *41*, 157-167.

[11] Weigend, F.; Ahlrichs, R. Balanced Basis Sets of Split Valence, Triple Zeta Valence and Quadruple Zeta Valence Quality for H to Rn: Design and Assessment of Accuracy. *Phys. Chem. Chem. Phys.* **2005**, *7*, 3297-3305.

[12] Weigend, F. Accurate Coulomb-Fitting Basis Sets for H to Rn. *Phys. Chem. Chem. Phys.* **2006**, *8*, 1057-1065.

[13] Alecu, I. M.; Zheng, J.; Zhao, Y.; Truhlar, D. G. Computational Thermochemistry: Scale Factor Databases and Scale Factors for Vibrational Frequencies Obtained from Electronic Model Chemistries. *J. Chem. Theory Comput.* **2010**, *6*, 2872-2887.

[14] Cavanagh, R. R.; Yates, J. T. Site Distribution Studies of Rh Supported on Al_2O_3-An Infrared Study of Chemisorbed CO. *J. Chem. Phys.* **1981**, *74*, 4150-4155.

[15] Yates, J. T.; Duncan, T. M.; Vaughan, R. W. Infrared Spectroscopic Study of Activated Surface Processes: CO Chemisorption on Supported Rh. *J. Chem. Phys.* **1979**, *71*, 3908-3915.

[16] Matsubu, J. C.; Yang, V. N.; Christopher, P. Isolated Metal Active Site Concentration and Stability Control Catalytic CO_2 Reduction Selectivity. *J. Am. Chem. Soc.* **2015**, *137*, 3076-3084.
[17] Ravel, B.; Newville, M. ATHENA, ARTEMIS, HEPHAESTUS: data analysis for X-ray absorption spectroscopy using IFEFFIT. *J. Synchrotron Radiat.* **2005,** *12,* 537-541.
[18] Ankudinov, A. L.; Ravel, B.; Rehr, J. J.; Conradson, S. D. Real-space multiple-scattering calculation and interpretation of x-ray-absorption near-edge structure. *Phys. Rev. B* **1998,** 58, 7565-7576.